Article

Combined Thermal Runaway Investigation of Coin Cells with an Accelerating Rate Calorimeter and a Tian-Calvet Calorimeter

Wenjiao Zhao [1], Magnus Rohde [2],*, Ijaz Ul Mohsin [2], Carlos Ziebert [2], Yong Du [3] and Hans J. Seifert [2]

[1] Volkswagen AG, 38239 Salzgitter, Germany; wanjiao.zhao@volkswagen.de
[2] Institute for Applied Materials-Applied Materials Physics, Karlsruhe Institute of Technology, 76344 Eggenstein, Germany; ijaz.mohsin@kit.edu (I.U.M.); carlos.ziebert@kit.edu (C.Z.); hans.seifert@kit.edu (H.J.S.)
[3] State Key Lab of Powder Metallurgy, Central South University, Changsha 410083, China; yong-du@csu.edu.cn
* Correspondence: maguns.rohde@kit.edu; Tel.: +49-7216-0824-328

Abstract: Commercial coin cells with $LiNi_{0.6}Mn_{0.2}Co_{0.2}O_2$ positive electrode material were investigated using an accelerating rate calorimeter and a Tian-Calvet calorimeter. After cycling and charging to the selected states of charge (SOCs), the cells were studied under thermal abuse conditions using the heat-wait-seek (HWS) method with the heating step of 5 K and a threshold for self-heating detection of 0.02 K/min. The onset temperature and the rate of the temperature rise, i.e., the self-heating rate for thermal runaway events, were determined. The morphology of the positive electrode, negative electrode and the separator of fresh and tested cells were compared and investigated with scanning electron microscopy (SEM). Furthermore, the microstructure and the chemical compositions of the individual components were investigated by X-ray diffraction (XRD) and inductively coupled plasma with optical emission spectrometry (ICP-OES), respectively. In the Tian-Calvet calorimeter, the coin cells with the selected SOCs and the individual components (positive electrode, negative electrode and separator) were heated up with a constant heating rate of 0.1 °C/min (ramp heating mode). Simultaneously, the heat flow signals were recorded to analyze the heat generation. The combination of the three different methods—the HWS method using the ES-ARC, ramp heating mode on both cells and the individual components using the Tian-Calvet calorimeter—together with a post-mortem analysis, give us a complete picture of the processes leading to thermal runaway.

Keywords: lithium-ion cells; thermal runaway; accelerating rate calorimeter; C80 Tian-Calvet calorimeter; thermal properties

1. Introduction

In the field of electric vehicles (EVs), as well as electric devices, Li-ion batteries (LIBs) are increasingly being adopted as mobile electric suppliers, due to their high capacity, long cycle life and high energy density [1–3]. The active material in the positive electrode mainly determines the performance, such as the specific energy, the capacity, the working voltage and the cycle life of batteries. Recently, the Ni-rich layered positive electrode material $LiNi_xMn_yCo_zO_2$ (NMC) has become one of the most promising positive electrode materials because of its high capacity and low cost compared to $LiCoO_2$ [4–6]. In the application of LIBs, the short circuit, charging/discharging with high current and/or high ambient temperature, can cause overheating and/or thermal non-uniformity in the battery pack, which can lead to thermal runaway, fire and explosion [7–15]. Therefore, it is essential to understand the thermal runaway process of LIBs in detail.

In a number of studies, it has been demonstrated that calorimetric methods are able to reveal important new insights into the reactivity, thermal behavior and safety of Li-ion batteries. Ma et al. [16] applied accelerating rate calorimetry (ARC) to investigate the impact of different electrolyte additives on the electrode/electrolyte reactivity in NMC-graphite cells. This investigation was further extended by Huang et al. [17] with ARC

measurements, who demonstrated the influence of the upper cut-off potential and the sample morphology on the thermal stability of NMC compounds. Important trade-offs have been identified between different Li[Ni$_x$Mn$_y$Co$_z$]O$_2$ grades using ARC up to higher temperatures [18] in order to determine the influence of the Ni content on reactivity and safety. A combination of ARC, X-ray diffraction and electrochemical measurements were used by Zhang et al. [19] to study the reactivity of NMC materials in contact with the electrolyte at elevated temperatures. The thermal failure of a commercial 18,650 battery with a NMC622 cathode was analyzed by ARC [20], while the morphological changes due to the thermal runaway were investigated by applying X-ray computed tomography (CT).

In a recent work, Shurtz [21] demonstrated that results from calorimetry measurements and thermodynamic calculations can constitute the basis for advanced thermal runaway models which are able to predict the heat release from layered metal oxide cathodes in contact with organic electrolytes.

In this work, the thermal behavior during thermal runaway events of commercial coin cells with positive electrode material LiNi$_{0.6}$Mn$_{0.2}$Co$_{0.2}$O$_2$ (NMC 622) were investigated by an accelerating rate calorimeter (ES-ARC, Thermal Hazard Technology, Bletchley, United Kingdom) [22,23] and a Tian-Calvet calorimeter (C80, Setaram Instruments, Lyon, France) [24]. Fresh and tested commercial coin cells were disassembled in a glovebox and the individual components of the coin cell (positive electrode, negative electrode and separator) were investigated with the C80 calorimeter in terms of thermal properties in the early stage of thermal runaway. Additionally, the chemical composition of the pristine materials was determined by inductively coupled plasma with optical emission spectrometry (ICP-OES) and the crystal structure as well as the morphology of the samples were investigated by X-ray diffraction (XRD) and scanning electron microscopy (SEM), respectively.

2. Experimental

The investigated coin cells are commercially available with lithium transition metal oxide NMC as active material in the positive electrode and graphite in the negative electrode. The dimensions of the coin cells are 14 mm in diameter and 5.4 mm in height. The nominal capacity of 85 mAh was defined by discharging at 0.2 C (1 C amounts to 85 mA) from 4.2 V to 3.0 V at 20 °C. The standard charge method was constant current constant voltage (CCCV) at 0.5 C from 3.0 V to 4.2 V. The charging and discharging process, respectively, were only applied to set the SOC; the cells were not cycled. However, the heat generation during cycling was studied by the authors in a previous study [25]. The weight of the coin cell is 2.4 ± 0.2 g on average. The electrodes are coated on both sites of the current collectors. The stripes of the coated current collector with the separator foil in between are spirally wound into a jellyroll form.

The thermal runaway measurements were carried out by using ES-ARC. The measurement temperature is set up in the range of 30–450 °C, and the detection threshold for thermal runaway reactions is 0.02 K/min. ES-ARC heats up the sample stepwise by 5 K and then holds the temperature for 30 min, which is the so-called wait mode to stabilize the measuring system. At the end of the wait mode the seek mode starts in which the rate of temperature change (dT/dt) is determined and compared with the set sensitivity of 0.02 K/min. If the rate of temperature increase dT/dt is lower than 0.02 K/min, the heat mode will be activated again. The heat-wait-seek loop terminates when the sample temperature reaches the set temperature of 450 °C or dT/dt exceeds 0.02 °C/min. In the first case, the system switches to the cooling mode, and in the second case, the calorimeter switches to the exotherm mode. In the exotherm mode the temperature difference between the sample cell and the heated walls of the calorimeter chamber, which are measured by the bomb sensor and the middle sensor, respectively, are driven to zero by controlling the heaters around the calorimeter. K-type thermocouples (Omega Newport Electronics GmbH, Deckenpfronn, Germany) were used as temperature sensors (Bomb sensor in Figure 1). The set-up of the thermal runaway measurement is shown in Figure 1. The test cell was

attached to the sample holder with heat resistant tape (3M industrial business, St. Paul, MN, USA). The temperature sensor was fixed to the surface of the cell.
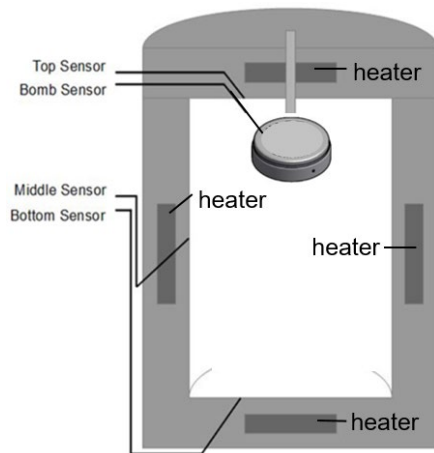

Figure 1. Schematic set-up for the thermal runaway measurement in the ARC.

Before the calorimetric measurements, the cells were at first fully charged to a 100% state of charge (SOC100), and then discharged to 50% (SOC50) and 0% (SOC0), respectively. The thermal runaway measurements were performed on three cells for each SOC level. The SOC level was estimated on discharge using a simple coulomb counting method [26], represented by the following equation:

$$SOC(t) = SOC(t-1) + \frac{I(t)}{Q} \cdot \Delta t \tag{1}$$

where $SOC(t)$ is the current SOC level, $SOC(t-1)$ the start SOC level, $I(t)$ the discharge current, Δt the time interval and Q the rated capacity. Starting from SOC100, the cell with a capacity of 85 mAh was discharged with constant current of 42.5 mAh for 1 h to SOC50, while discharging for 2 h with the same current was used to set SOC0.

Thermal characterization was performed on the individual components, i.e., separator foil, cathode and anode sheet, respectively, using the C80 calorimeter. The measuring temperature range was from 60 °C to 150 °C with a scanning rate 0.1 °C/min. The highest temperature was selected below the onset of uncontrollable self-heating of the cells. Not only the full cells but also the individual components sealed in crucibles were investigated by the C80 calorimeter. For the preparation of these measurements, a fresh cell was disassembled in a glovebox followed by washing of the separator and the positive and the negative electrode with Dimethyl Carbonate (DMC) with a purity of 99%, and then by drying for 24 h at room temperature under a vacuum condition. Positive and negative electrodes with 15 μL electrolyte of 1 M $LiPF_6$ in 1:1 (by weight) EC/DMC (LP30, BASF, Ludwigshafen, Germany) were sealed into crucibles in a glovebox. The two set-ups are shown in Figure 2, where the shield-lids are located above the vessels to optimize thermal isolation. The set-up on the left side of Figure 2 was used for the complete coin cell while the set up shown on the left side was applied for the thermal analysis of the individual components of the cell. Tested cells were charged to SOC100, SOC50 and SOC0.

The chemical composition of the positive and negative electrodes was investigated quantitatively by inductively coupled plasma with optical emission spectrometry (ICP-OES). Approximately 5 mg of the specimen was dissolved in a mixture of 6 mL hydrochloric acid and 2 mL nitric acid, at 80 °C for four hours. To measure transition metal elements (Ni, Co, Mn) and Li, the chemical digestion solution was diluted and an internal standard solution was added, which were a constant amount of scandium and sodium solution, respectively. The XRD measurements were performed in the angle range of 10°–90°, with a step size increment of 0.01°, and the data were collected 360 s/step. The morphology of

the electrodes and separator were observed by a scanning electron microscope, FEI XL30S (Philips, Eindhoven, Netherlands). The separator was sputtered with a gold film before the measurement. The cathode and the anode were observed by a JEOL JSM-840 scanning electron microscope with a tungsten cathode.
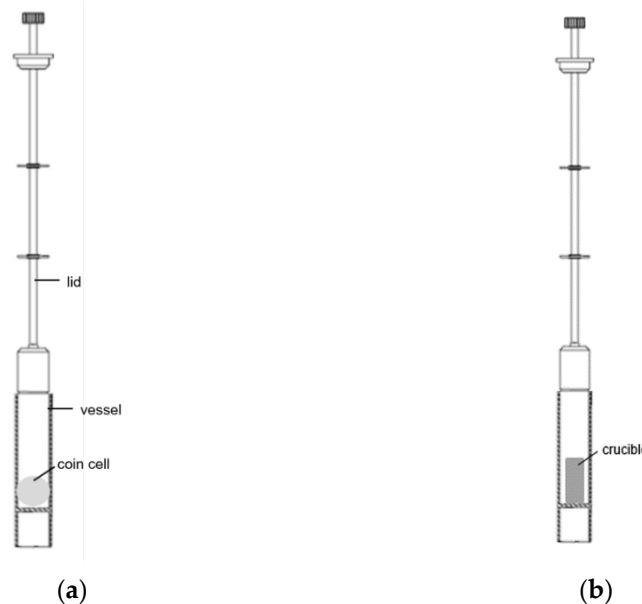

(**a**)   (**b**)

Figure 2. Schematic set-ups for the temperature measurement of full cell (**a**) and individual components (**b**) in the C80 calorimeter [18].

3. Results and Discussion

3.1. Results of Thermal Runaway Investigation Using ES-ARC

From the ARC measurements, the thermal behavior at various SOCs was studied regarding rates of temperature increase and the onset temperature of the thermal runaway. During the measurements on fully charged coin cells, which are shown in Figure 3, maximum temperatures during thermal runaway exceeded 450 °C, which corresponds to the level above which the ARC starts to actively cool down by pressurized air.
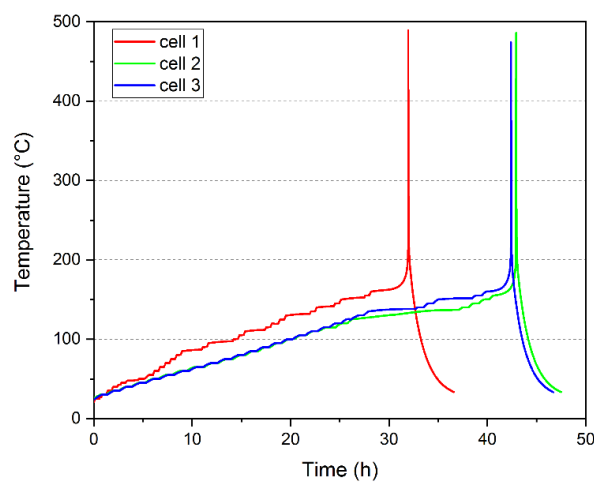

Figure 3. Temperature changes vs. time during HWS measurements of three cells with SOC100 measured by ES-ARC.

Maximum temperature levels around 490 °C were reached for the three coin cells studied. The time difference between the measurement of Cell 1 and measurements of Cell 2 and Cell 3 was due to the higher heating power in the measurement of Cell 1 compared to

that of Cell 2 and of Cell 3. The 5 K steps were faster than Cell 2 and Cell 3, since the longer heating time resulted in more stable and reproducible measurements. However, the overall results for the maximum temperature and the onset temperatures were not affected by the increased waiting time.

The onset temperatures for strong self-heating exothermic reactions could be observed at 164 °C, 157 °C and 161 °C, respectively (Figure 4), where the temperature increasing rate is above the threshold sensitivity of 0.02 °C/min. The uncontrollable self-heating heated the cells with temperature increasing rates of over 10 °C/min. Therefore, these temperatures can be taken as the onset of thermal runaway events. As already mentioned above, the larger heating power during the measurement of Cell 1 led to temperature increasing rates above the threshold sensitivity which could not be reproduced in cases of Cells 2 and 3. However, the temperature increasing rates in the measurement of Cell 2 and 3 below onset temperature revealed small exothermic reactions during heating, which could be due to the decomposition of the solid electrolyte interface (SEI) layer [13] or the exothermic reactions between electrolyte [27] and electrodes. The possible reactions and their temperatures were described in [28].
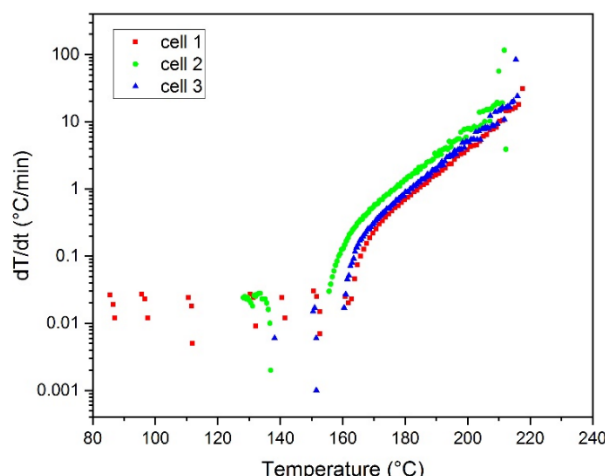

Figure 4. dT/dt-curves vs. temperature in exothermal mode of three cells with SOC100 measured by ES-ARC.

With decreasing SOC, the thermal effects become less violent and intense. The thermal runaway events on coin cells with SOC100 reached 480 °C with a temperature increasing rate up to 100 °C/min, while in the case of SOC50, the onset temperature increased to 193 °C. The maximum temperatures were 271 °C, 299 °C and 320 °C for the three cells (Figure 5). Before the thermal runaway, small exothermic reactions were observed at approximately 181 °C and 171 °C on Cell 2 and Cell 3 (Figure 6). It is also worth noticing that the shape of the temperature rate curve shows a decelerating trend after reaching the maximum rate of 110 °C/min. The cells with SOC0 show even much more controllable thermal behavior. The maximum temperatures of all tested cells were below 230 °C (Figure 7), and during the evolution of the exothermic effects, temperature increasing rates smaller than 1 °C/min were detected (Figure 8). The onset temperature of the exothermic effects was about 199 °C on average. The self-heating effects of the tested cells terminated at 217 °C, 223 °C and 212 °C, respectively. The shape of the temperature rate curve was similar to that of SOC50, but in a much lower range (<1 °C/min). These results imply that cells with lower SOCs are thermally more stable.
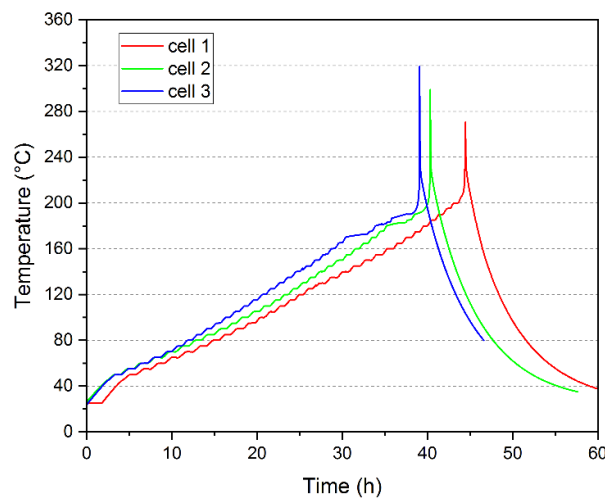
Figure 5. Temperature changes vs. time during HWS measurements of three cells with SOC50 measured by ES-ARC.
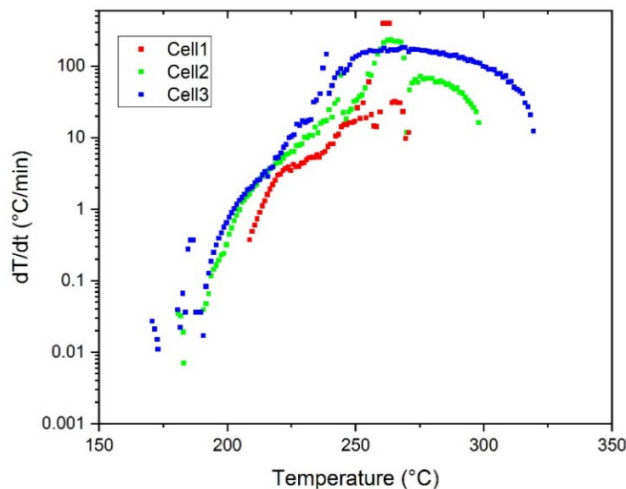

Figure 6. dT/dt-curves vs. temperature in exothermal mode of three cells with SOC50 measured by ES-ARC.
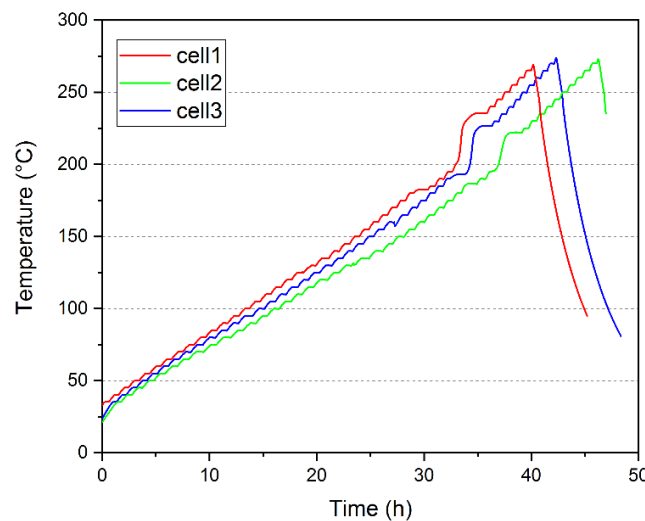

Figure 7. Temperature changes vs. time during HWS measurements of three cells with SOC0 measured by ES-ARC.
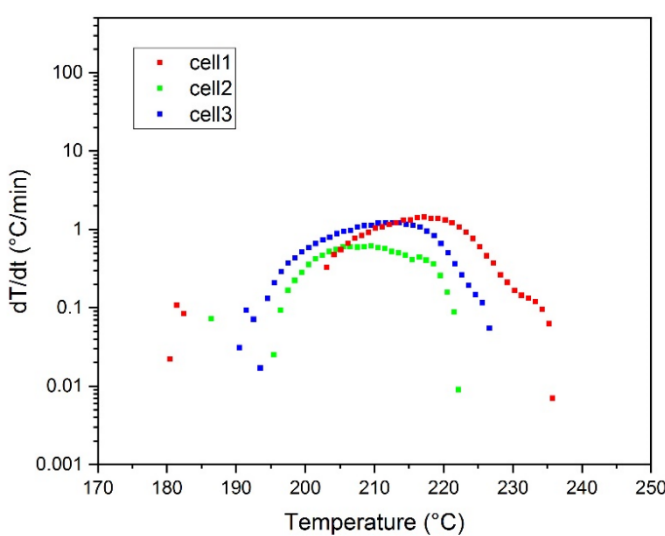
Figure 8. dT/dt-curves vs. temperature in exotherm mode of three cells with SOC0 measured by ES-ARC.

The XRD analysis reveals the phase transition during thermal runaway events, as shown in Figure 9. In a fresh cell, the positive electrode material exhibits a layered structure with space group $R\bar{3}m$ (No.166) [29,30], and the conducting additive, i.e., carbon, is observed in the diffraction pattern. The XRD pattern of the negative electrode shows that it consists of graphite coating on a Cu foil. When the cell was heated up to 126 °C, no decomposition was observed at the positive electrode. After three times of cycling and being charged to SOC100, lithium ions could be found intercalated at the negative electrode in the XRD pattern (Figure 9b). The positive electrode was therefore de-lithiated as Li_xMO_2 (M represents Ni, Co and Mn) with x < 1. After the thermal runaway measurement up to 450 °C, the de-lithiated positive electrode material had transformed completely from a layered structure to a rock-salt structure. Dahn et al. [31] proposed that the de-lithiated layered structure Li_xCoO_2 (x < 1) positive electrode material would thermally decompose to the rock-salt structure Co_3O_4 and release oxygen. Further studies [32–34] showed by a detailed investigation of the thermal stability of de-lithiated positive electrode materials that these processes of phase transformation and thermal decomposition also take place in NMC and NCA.

In the SEM images of heat-treated positive electrode (Figure 10b,c), cracks on the particles (yellow circles) are visible. The particles of the negative electrodes established a relative stable form after heating to 126 °C and 450 °C. However, there seems to be an increasing surface roughness induced by the exposition to higher temperatures (Figure 11), which could have been result of the reactions with the electrolyte or the effect of a decomposition.

An EDX analysis was not carried out due to technical reasons related to the handling of powdered samples in the SEM. However, an analysis of the element distribution was conducted by an integral chemical analysis (ICP-OES) of the electrode sheets. While the heating of the cathode and anode sheets, respectively, up to 126 °C did not result in significant change in the distribution of the elements, further heating to 450 °C induced a reduction in the oxygen content in the cathode as well as a loss of Li and carbon in the anode. These results are consistent with the XRD data shown in Figure 9, which indicate that up to 126 °C the cathode as well as the anode remains stable, but that heating to 450 °C leads to a decomposition of the NMC622 phase in the cathode and to a loss of the LiC phases in the anode.

The morphology of the separator, which consists of a three-layer polymer foil with polyethylene (PE) sandwiched between two polypropylene layers (PP), is shown in Figure 12. Under heating up to 126 °C, a partial closing of the pores can be observed which can stop the Li-ion transport through the electrolyte and thereby prevent short

circuiting. In addition, some sub-micron-sized particles fractured from the cathode material agglomerates were found to attach on the separator, which might be an indication of the beginning decomposition of the electrodes or electrolyte, respectively. Although the surface temperature of the cell was 126 °C, the internal temperature could reach the melting point of polypropylene 130 °C, so that the separator started to melt (Figure 12b). It is also probable that due to the partial crystallinity of PP, the glassy phase becomes softer approaching the melting temperature. An optical inspection of the separator after heating to 126 °C showed no significant changes in colour or shrinkage of the polymer foil. However, the mechanical integrity seemed to be affected by the heat treatment.

Heating up to 450 °C caused a complete decomposition of the PP/PE/PP layer system. The decomposition of PP starts at 200 °C and is completed at about 350 °C [35]. The degradation of PE occurs between 300 °C and 500 °C [35]. Therefore, the separator is completely pyrolyzed at temperatures around and above 450 °C.
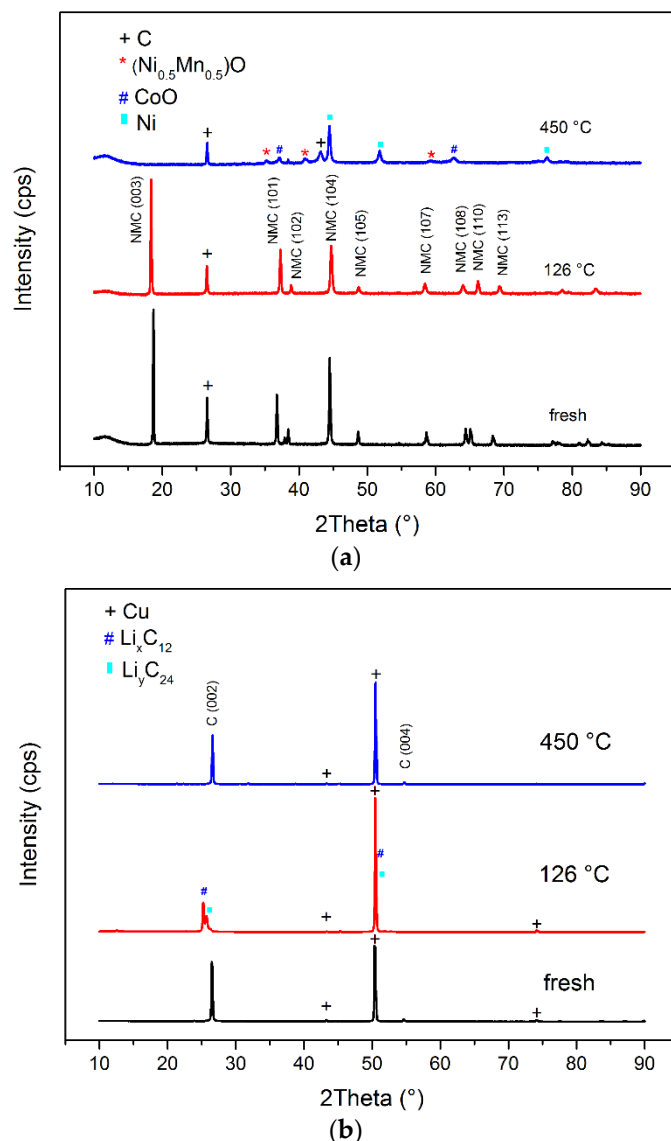

Figure 9. XRD patterns of the electrodes for the fresh cell, after heating to 126 °C and after heating to 450 °C: (**a**) cathode, (**b**) anode.
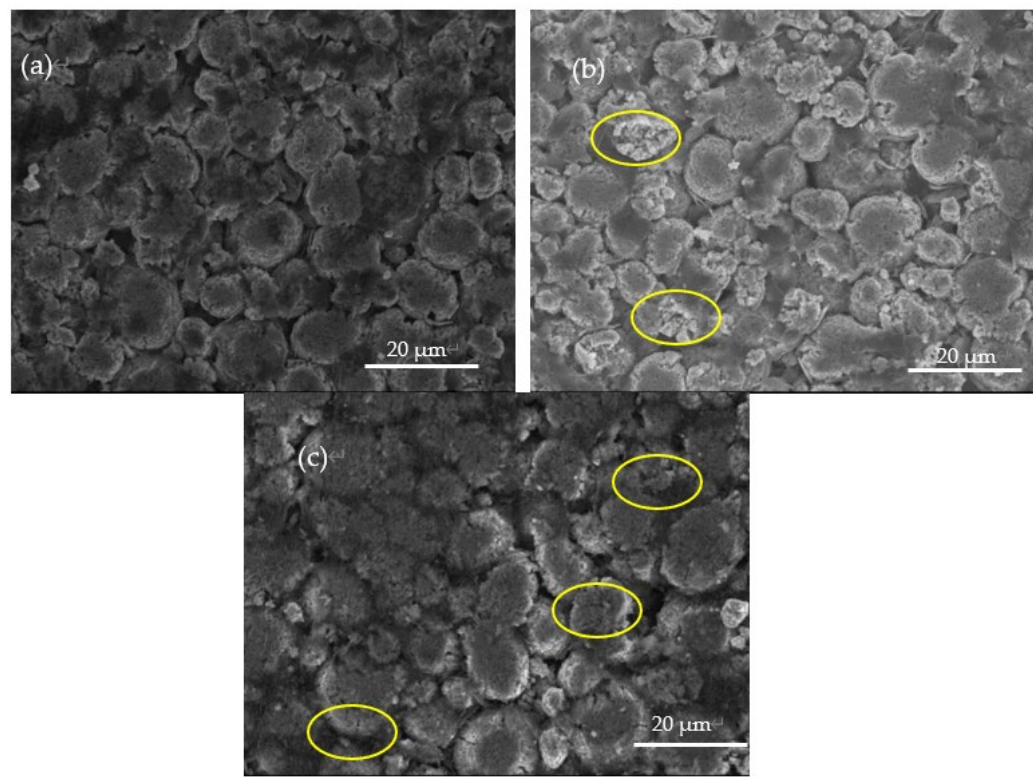
Figure 10. SEM images of the positive electrodes from (**a**) a fresh cell, (**b**) the cell heated up to 126 °C, (**c**) the cell heated up to 450 °C.
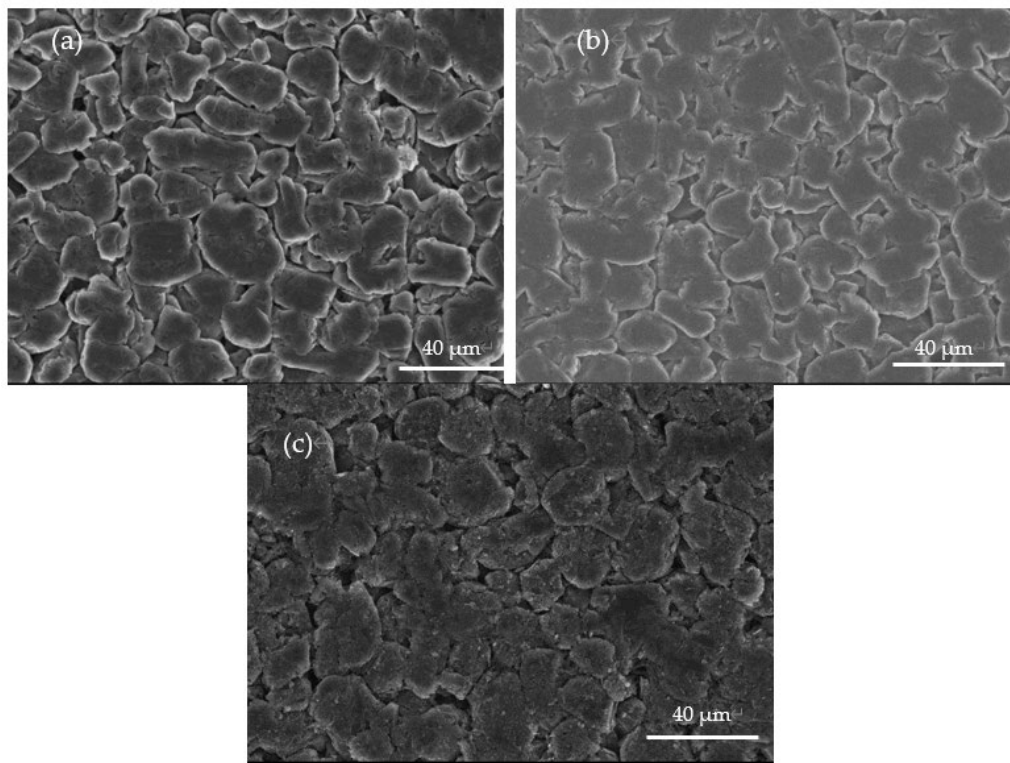

Figure 11. SEM images of the negative electrodes from (**a**) a fresh cell, (**b**) the cell heated up to 126 °C, (**c**) the cell heated up to 450 °C.
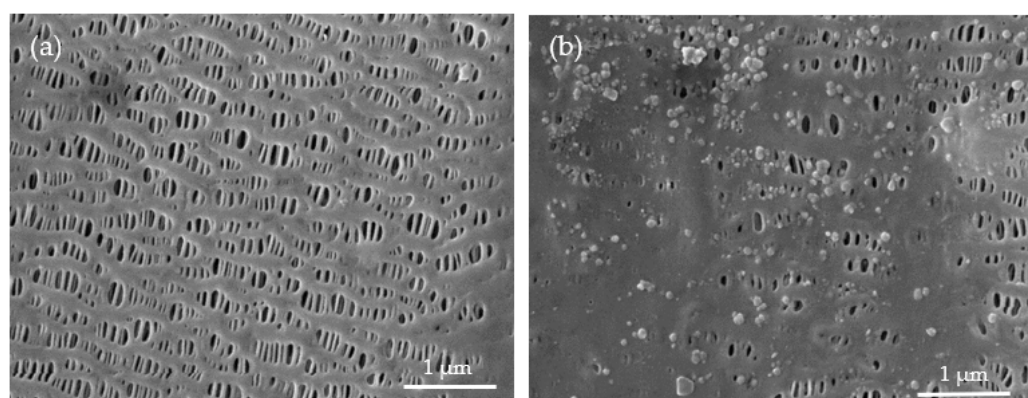
Figure 12. SEM images of the separators from (**a**) a fresh cell, (**b**) the cell heated up to 126 °C.

3.2. Early Stages of Thermal Runaway Investigated by a C80 Calorimeter

In order to develop a more detailed insight into the thermal runaway events, the early stages of thermal runaway were studied by a sensitive Tian-Calvet calorimeter (C80). For safety concerns, the maximum measuring temperature in the C80 was set to 150 °C, which is just below the onset temperature of thermal runaway. As previous thermal behavior studies on LIBs [28,36,37] revealed, the reactions below 150 °C are mainly caused by the thermal instability of liquid electrolyte and intercalated lithium ions in the negative electrode. Therefore, the full cells as well as the individual components with electrolyte were investigated by a C80 calorimeter below this temperature level.

A temperature scan in the C80 calorimeter from 60 °C to 150 °C with a heating rate of 0.1 °C/min is shown in Figure 13 for the full cell and the single components. Before the measurement, the cell was charged to SOC100. The single electrodes were measured in contact with the LP30 liquid electrolyte (LiPF$_6$ in EC/DMC). In the measurement of the full cell, no exothermic reactions were detected. This might be due to the fact that the electrolyte of coin cells contains stabilizing additives and is therefore more thermally stable than LP30. The relatively strong endothermic heat effect between 130 and 135 °C can be explained by the melting of the separator. This corresponds to the results of the temperature scan of the single separator. In the thermal analysis of the separator, the endothermic heat effect due to the melting of polyethylene was observed at 132.4 $\pm$ 2.5 °C. The melting enthalpy was 33.9 $\pm$ 1.9 J/g. These results are comparable to the data in the literature [38]: the onset temperature of the melting of polyethylene was 135 $\pm$ 1 °C with a melting enthalpy of 32.4 J/g. No thermal effect was found on the positive electrode by heating up to 150 °C, which is probably due to the de-lithiated state, while the negative electrode showed a series of exothermic heat effects.

For a more detailed analysis of the temperature scan of the single negative electrode, the electrode was fitted to a series of Gaussian peaks which allows a deconvolution of the calorimeter trace. The results of the fit are shown in Figure 14 together with the single Gaussian peaks used in the fitting procedure.

The first exothermic heat effect on the negative electrode was observed at approximately 72 °C, as heat flow rate is exhibited in Figure 14. Although the SEI was probably partially removed by the washing and drying process, an SEI decomposition reaction can be detected via an exothermic heat effect [39]. The exothermic heat due to SEI decomposition was 0.044 J/g. The thermal stability of EC is higher than DMC due to its stronger binding energy of the covalent bond in the cyclic carbonate [40]. The exothermic peaks at 85 °C, 95 °C and 108 °C are supposed to be the reactions between LiC6 and DMC [41]. At approximately 120 °C, the exothermic peak due to the reaction of intercalated lithium ions and EC was observed, which is in a good agreement with the literature [41]. Based on the computed curve, the heat generations in the negative electrode due to reactions of DMC and EC were 504.2 J/g and 90.4 J/g, respectively. Due to the sensitivity of the C80 calorimeter, it should be also possible to study the effects of electrolyte additive. It has been shown in an ARC

study [16] that additives such as vinylene carbonate (VC), fluoroethylene carbonate (FEC) and vinyl ethylene carbonate (VEC) can influence thermal effects in NMC/graphite cells and give additional information about changes in the reactivity of the electrodes. However, this was beyond the scope of this paper.
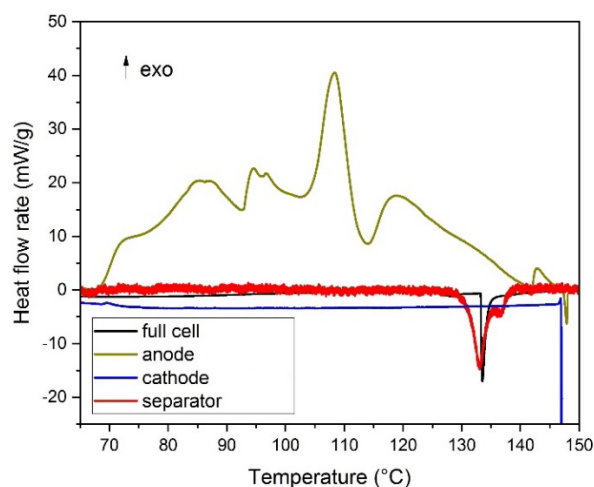

Figure 13. The heat flow rate of the full cell and the single components versus the temperature.
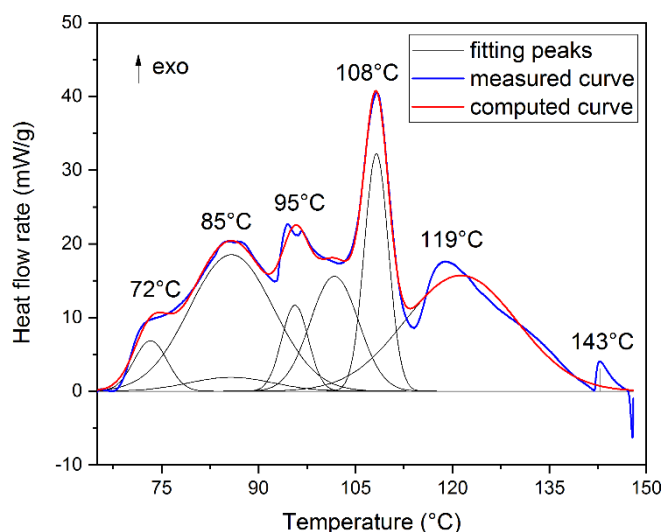

Figure 14. The measured heat flow rate, the fitting peaks and the computed curve for the negative electrode and electrolyte with SOC100.

The heat flow rates of the negative electrodes from a fresh cell, the cell with SOC0 and the cell with SOC100 are compared in Figure 15. The SOC50 cell was not included in the measurements of the heat flow rates since the focus was on the extremal cases SOC0 and SOC 100 compared to the fresh cell with a state of charge below 10%. The exothermic effect due to the SEI decomposition of SOC0 and SOC100 was larger compared to the fresh cell, which could be explained by the continuous growth of the SEI layer [37] during cycling and aging. The peaks of the SEI decomposition appear in a small temperature interval for the SOC0-cell (71 °C), SOC100-cell (69 °C) and fresh cell (69 °C), respectively. In the temperature range of 108–150 °C, there are a number of small exothermic peaks on the curve for the fresh cell. Since the lithium-ion content is much smaller than in the fully charged cell, which can be estimated to be lower than SOC10, the heat effects were noticeably smaller. In the case of the cell with SOC0, heat effects in the heat flow rate could not be observed at temperatures above 75 °C.
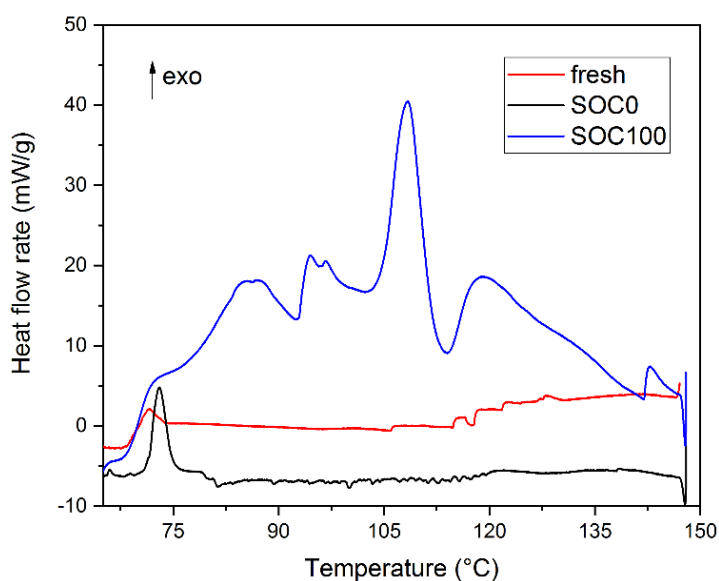
Figure 15. The heat flow rates of the negative electrodes with SOC100, SOC0 and fresh cells vs. the temperature.

4. Conclusions

This work combined an ES-ARC and a C80 calorimeter in order to provide a novel approach for studying the thermal properties of Li-ion coin cells at high temperature. While the ARC allows for the measurement of the complete thermal runaway, including the final self-heating event, with very high temperature increasing rate, the C80 calorimeter gives a higher resolution of the thermal effects in the early stages. The onset temperature of the thermal runaway was approximately 161 °C for the cells with SOC100. It could be shown by XRD that during thermal runaway, the de-lithiated layered structure positive electrode transforms and decomposes into a rock-salt structure. The cells were self-heated to over 450 °C, and the maximum temperature increasing rate reached 100 °C/min. With lower SOCs, the cells showed a more stable thermal behavior with higher onset temperature. The temperature increasing rate of the cells with SOC0 was even below 1 °C/min. In the early stage of thermal runaway below 150 °C, the intercalated lithium ions at the negative electrode dominated the heat generation. However, this exothermic effect was also reduced at lower SOC levels because the fraction of lithium was decreased. The de-lithiated positive electrode NMC material $LixNi_{0.6}Mn_{0.2}Co_{0.2}O_2$ was stable below 150 °C, and no phase transition or heat effect was observed.

From the result of our calorimetric measurement the following conclusions with regard to the safety of NMC622/graphite cells can be drawn:

The thermal effects up to 150 °C are relatively small and self-heating effects and can be neglected due to very small heat flow rates coupled with rates of temperature change below a level of 0.1 °C/min. Therefore, monitoring of the temperature rate can be an additional measure for a safe operation.

The highest state of charge sets the lowest onset temperature for self-heating effects. Therefore, reducing the SOC by discharging leads to increasing onset temperature and can prevent thermal runaway.

The three-layered PP/PE/PP separator is able to interrupt ion flow in the electrolyte by closing pores during softening and melting in the temperature range from 125 to 140 °C. Since the melting is an endothermal effect, heat is dissipated or absorbed and forces a thermal stabilization of the cell.

M.R., C.Z., I.U.M., Y.D. and H.J.S.; visualization, W.Z. and I.U.M.; supervision, C.Z., M.R., Y.D. and H.J.S.; project administration, H.J.S. and Y.D.; funding acquisition, H.J.S. and Y.D. All authors have read and agreed to the published version of the manuscript.

Institutional Review Board Statement: Not applicable.

Informed Consent Statement: Not applicable.

Data Availability Statement: The data presented in this study are available on request from the corresponding author.

Conflicts of Interest: The authors declare no conflict of interest. The funders had no role in the design of the study; in the collection, analyses, or interpretation of data; in the writing of the manuscript; or in the decision to publish the results.

References

1. Kurzweil, P. *Electrochemical Energy Storage for Renewable Sources and Grid Balancing*; Moseley, P.T., Garche, J., Eds.; Elsevier: Amsterdam, The Netherlands, 2015; Chapter 16; pp. 269–307.
2. Ren, G.; Ma, G.; Cong, N. Review of electrical energy storage systems for vehicular applications. *Renew. Sustain. Energy Rev.* **2015**, *41*, 225–236. [CrossRef]
3. Wang, Y.; Liu, Q.; Li, S.; Cartmell, S.; Ferrara, Z.; Deng, D.; Xiao, J. Lithium and lithium-ion batteries for applications in microelectronic devices: A review. *J. Power Sources* **2015**, *286*, 330–345. [CrossRef]
4. Yabuuchi, N.; Ohzuku, T. Novel lithium insertion material of $LiCo_{1/3}Ni_{1/3}Mn_{1/3}O_2$ for advanced lithium-ion batteries. *J. Power Sources* **2003**, *119*, 171–174. [CrossRef]
5. Wang, Y.D.; Jiang, J.W.; Dahn, J.R. The reactivity of delithiated $Li(Ni_{1/3}Co_{1/3}Mn_{1/3})O_2$, $Li(Ni_{0.8}Co_{0.15}Al_{0.05})O_2$ or $LiCoO_2$ with non-aqueous electrolyte. *Electrochem. Commun.* **2007**, *9*, 2534–2540. [CrossRef]
6. MacNeil, D.D.; Lu, Z.; Dahn, J.R. Structure and electrochemistry of $Li(Ni_xCo_{1-2x}Mn_x)O_2$ ($0 \le x \le 1/2$). *J. Electrochem. Soc.* **2002**, *149*, A1332. [CrossRef]
7. Saito, Y.; Takano, K.; Negishi, A. Thermal behaviors of lithium-ion cells during overcharge. *J. Power Sources* **2001**, *97–98*, 693–696. [CrossRef]
8. Spotnitz, R.; Franklin, J. Abuse behavior of high-power, lithium-ion cells. *J. Power Sources* **2003**, *113*, 81–100. [CrossRef]
9. Armand, M.; Tarascon, J.M. Building better batteries. *Nature* **2008**, *451*, 652–657. [CrossRef]
10. Goodenough, J.B.; Kim, T. Challenges for Rechargeable Li Batteries. *Chem. Mater.* **2010**, *22*, 587–603. [CrossRef]
11. Thackeray, M.M.; Wolverton, C.; Isaacs, E.D. Electrical energy storage for transportation—Approaching the limits of, and going beyond, lithium-ion batteries. *Energy Environ. Sci.* **2012**, *5*, 7854–7863. [CrossRef]
12. Balakrishnan, P.; Ramesh, R.; Kumar, P. Safety mechanisms in lithium-ion batteries. *J. Power Sources* **2006**, *155*, 401–414. [CrossRef]
13. Wang, Q.; Ping, P.; Zhao, X.; Chu, G.; Sun, J.; Chen, C. Thermal runaway caused fire and explosion of lithium ion battery. *J. Power Sources* **2012**, *208*, 210–224. [CrossRef]
14. Golubkov, A.W.; Fuchs, D.; Wagner, J.; Wiltsche, H.; Stangl, C.; Fauler, G.; Voitic, G.; Thaler, A.; Hacker, V. Thermal-runaway experiments on consumer Li-ion batteries with metal-oxide and olivin-type cathodes. *RSC Adv.* **2014**, *4*, 3633–3642. [CrossRef]
15. Yeow, K.F.; Teng, H. Characterizing Thermal Runaway of Lithium-ion Cells in a Battery System Using Finite Element Analysis Approach. *SAE Int. J. Altern. Powertrains* **2013**, *2*, 179–186. [CrossRef]
16. Ma, L.; Xia, J.; Xia, X.; Dahn, J.R. The Impact of Vinylene Carbonate, Fluoroethylene Carbonate and Vinyl Ethylene Carbonate Electrolyte Additives on Electrode/Electrolyte Reactivity Studied Using Accelerating Rate Calorimetry. *J. Electrochem. Soc.* **2014**, *161*, A1495–A1498. [CrossRef]
17. Huang, Q.; Liu, L.M.A.; Ma, X.; Li, J.; Wang, J.; Dahn, J.R. The reactivity of charged positive $Li_{1-n}[Ni_xMn_yCo_z]O_2$ electrodes with electrolyte at elevated temperatures using accelerating rate calorimetry. *J. Power Sources* **2018**, *390*, 78–86. [CrossRef]
18. Ma, L.; Nie, M.; Xia, J.; Dahn, J.R. A systematic study on the reactivity of different grades of charged $Li[Ni_xMn_yCo_z]O_2$ with electrolyte at elevated temperatures using accelerated rate calorimetry. *J. Power Sources* **2016**, *327*, 145–150. [CrossRef]
19. Zhang, N.; Li, J.; Li, H.; Liu, A.; Huang, Q.; Ma, L.; Li, Y.; Dahn, J.R. Structural, electrochemical, and thermal properties of Ni-rich $LiNi_xMn_yCo_zO_2$ materials. *Chem. Mater.* **2018**, *30*, 8852–8860. [CrossRef]

20. Patel, D.; Robinson, J.B.; Ball, S.; Brett, D.J.L.; Shearing, P.R. Thermal Runaway of a Li-Ion Battery Studied by Combined ARC and Multi-Length Scale X-ray CT. *J. Electrochem. Soc.* **2020**, *167*, 090511. [CrossRef]

21. Shurtz, R.C. A Thermodynamic Reassessment of Lithium-Ion Battery Cathode Calorimetry. *J. Electrochem. Soc.* **2020**, *167*, 140544. [CrossRef]

22. Wang, Y.; Shu, C. Hazard Characterizations of Liion Batteries: Thermal Runaway Evaluation by Calorimeter Methodology. In *Rechargeable Batteries*; Zhang, Z., Zhang, S., Eds.; Springer: Cham, Switzerland, 2015; pp. 419–454.

23. Thermal Hazard Technology. ARC Accelerating Rate Calorimetry. Available online: https://www.thermalhazardtechnology.com/contentfiles/downloads/38.pdf (accessed on 17 October 2021).

24. Zhao, W. Thermal Characterization of Lithium-Ion Cells with Positive Electrode Materials $LiNi_xMn_{0.8-x}Co_{0.2}O_2$ and Their Components. Ph.D. Thesis, Karlsruhe Institute of Technology, Karlsruhe, Germany, 2021; pp. 25–35. [CrossRef]

25. Zhao, W.; Rohde, M.; Mohsin, I.; Ziebert, C.; Seifert, H. Heat generation in NMC622 coin cells during electrochemical cycling: Separation of reversible and irreversible heat effects. *Batteries* **2020**, *6*, 55. [CrossRef]

26. Chang, W. The state of charge estimating methods for battery: A Review. *ISRN Appl. Math.* **2013**, *2013*, 953792. [CrossRef]

27. Lopez, C.F.; Jeevarajan, J.A.; Mukherjee, P.P. Characterization of Lithium-Ion Battery Thermal Abuse Behavior Using Experimental and Computational Analysis. *J. Electrochem. Soc.* **2015**, *162*, A2163–A2173. [CrossRef]

28. Melcher, A.; Ziebert, C.; Rohde, M.; Seifert, H.J. Modeling and Simulation of the Thermal Runaway Behavior of Cylindrical Li-Ion Cells—Computing of Critical Parameters. *Energies* **2016**, *9*, 292. [CrossRef]

29. Reimers, J.N.; Dahn, J.R. Electrochemical and insitu X-ray-diffraction studies of lithium intercalation in Li_xCoO_2. *J. Electrochem. Soc.* **1992**, *139*, 2091–2097. [CrossRef]

30. Labrini, M.; Saadoune, I.; Almaggoussi, A.; Elhaskouri, J.; Amoros, P. The $LiyNi_{0.2}Mn_{0.2}Co_{0.6}O_2$ electrode materials: A structural and magnetic study. *Mat. Res. Bull.* **2012**, *47*, 1004–1009. [CrossRef]

31. Dahn, J.R.; Fuller, E.W.; Obrovac, M.; von Sacken, U. Thermal-stability of Li_xCoO_2, Li_XNiO_2 and lambda-MnO_2 and consequences for the safety of Li-ion cells. *Solid State Ionics* **1994**, *69*, 265–270. [CrossRef]

32. Sharifi-Asl, S.; Soto, F.A.; Nie, A.; Yuan, Y.; Asayesh-Ardakani, H.; Foroozan, T.; Yurkiv, V.; Song, B.; Mashayek, F.; Klie, R.F.; et al. Facet-Dependent Thermal Instability in $LiCoO_2$. *Nano Lett.* **2017**, *17*, 2165–2171. [CrossRef]

33. Bak, S.-M.; Hu, E.; Zhou, Y.; Yu, X.; Senanayake, S.; Cho, S.-J.; Kim, K.-B.; Chung, K.Y.; Yang, X.-Q.; Nam, K.-W. Structural Changes and Thermal Stability of Charged $LiNi_xMn_yCo_zO_2$ Cathode Materials Studied by Combined In Situ Time-Resolved XRD and Mass Spectroscopy. *ACS Appl. Mater. Interfaces* **2014**, *6*, 22594–22601. [CrossRef]

34. Sharifi-Asl, S.; Lu, J.; Amine, K.; Shahbazian-Yassar, R. Oxygen Release Degradation in Li-Ion Battery Cathode Materials: Mechanisms and Mitigating Approaches. *Adv. Energy Mater.* **2019**, *9*, 1900551. [CrossRef]

35. Peterson, J.D.; Vyazovkin, S.; Wight, C.A. Kinetics of the Thermal and Thermo-Oxidative Degradation of Polystyrene, Polyethylene and Poly(propylene). *Macromol. Chem. Phys.* **2001**, *202*, 775–784. [CrossRef]

36. Wang, Q.; Sun, J.; Yao, X.; Chen, C. Thermal stability of $LiPF_6$/EC+DEC electrolyte with charged electrodes for lithium ion batteries. *Thermochim. Acta* **2005**, *437*, 12–16. [CrossRef]

37. Wang, Q.; Sun, J.; Yao, X.; Cheng, S.-C. Thermal Behavior of Lithiated Graphite with Electrolyte in Lithium-Ion Batteries. *J. Electrochem. Soc.* **2006**, *153*, A274–A329. [CrossRef]

38. Love, C.T. Thermomechanical analysis and durability of commercial micro-porous polymer Li-ion battery separators. *J. Power Sources* **2011**, *196*, 2905–2912. [CrossRef]

39. Zhuang, G.; Chen, Y.; Ross, P.N. The Reaction of Lithium with Dimethyl Carbonate and Diethyl Carbonate in Ultrahigh Vacuum Studied by X-ray Photoemission Spectroscopy. *Langmuir* **1999**, *15*, 1470–1479. [CrossRef]

40. Wang, Q.; Sun, J.; Chen, X.; Chu, G.; Chen, C. Effects of solvents and salt on the thermal stability of charged $LiCoO_2$. *Mater. Res. Bull.* **2009**, *44*, 543–548. [CrossRef]

41. Wang, Q.; Sun, J.; Chen, C. Effects of solvents and salt on the thermal stability of lithiated graphite used in lithium ion battery. *J. Hazard. Mater.* **2009**, *167*, 1209–1214. [CrossRef]